ER309L-Filled Dissimilar GTAW Joints between AISI 304 Stainless Steel and AISI 1010 Low-Carbon Steel

Philip Baidoo[1], Banabas N. Bediako[1], Emmanuel Obobi Tettefio[2] and Vivian Hinneh[3]

[1]Department of Mechanical and Automotive Technology Education, University of Skills Training and Entrepreneurship Development, Kumasi, Ghana
[2]Department of Mechanical Engineering, Ho Technical University, Ho, Ghana
[3]Department of Engineering, Mampong Technical College of Education, Mampong, Ghana

---***---

Abstract-*Since ancient times, welding technology has engaged in recreation a noteworthy protagonist in metal joining processes. This study investigated the effects of using a transitional filler material, ER309L, to join AISI 304 austenitic stainless steel and AISI 1010 low carbon steel (LCS) using Gas Tungsten Arc Welding (GTAW). The study aimed to evaluate the mechanical properties and microstructure of the welded joints. Weldment joints stood prepared using three filler materials, and their tensile properties, impact strength, hardness values and microstructures were determined. The TIG welding process uses a non-consumable tungsten electrode to generate the weld, which is protected from oxidation and contamination by an inert gas shield. The results revealed welds that were free from impurities and had a clean, high-quality appearance. The use of ER309L as a transitional filler material for joining AISI 304 austenitic stainless steel (ASS) and AISI 1010 low carbon steel positively influenced the mechanical and microstructural properties of the weldment, making it suitable for high-quality weld production in industries such as aerospace and automotive engineering.*

Keywords: **TIG Welding; transitional filler martial; Extensometer gauge length; material exhibits; Yield strength; Shielding Gas.**

Weldment has been started since ancient times. Humphry Davy discovered the electric arc by using a battery and two carbon electrodes. However, this has principles of gas metal arc weldment were developed after the invention of the electric generator [1]. The gas metal arc welding process is widely used nowadays in automobiles, railway construction, ship buildings, and nuclear power plants Metal can be transferred to the weld pool in three ways, such as globular type, short circuit type, and spray type. Pulsed spray metal transfer was introduced after as a modification of the spray metal transfer mode. Spray metal transfer was the first mode used in this process. Each type of metal transfer has its own influential with regards of usage, required arc current and weld penetration [2]. In dissimilar metal welding, filler metal plays an important role because its composition often differs from that of the parent metals. During welding, the parent metals and filler metal combine in a specific ratio to form the weld metal. Therefore, controlling the composition of the weld metal is essential when joining dissimilar metals. The weld metal composition can be determined based on the assumption that it is formed from a mixture of the parent metals and the filler metal [3].

In modern steel construction, it is sometimes necessary to produce durable dissimilar metal joints between low-alloy or carbon steel and stainless steel [4]. The automobile industry, pressure vessels and shipbuilding. The formation of intermetallic compounds makes the joining of dissimilar materials more difficult. During dissimilar metal welding, key factors such as weld metal, composition, dilution, melting temperature, thermal conductivity, and coefficient of thermal expansion, may lead to weld discontinuities [5]. The researchers intended to investigated Influence of ER309L filler Materials in Joining AISI304 ASS and AISI1010 LCS by using GTAW, also known as TIG welding. When a structure fails due to the loss of mechanical properties of weld metal, the financial and endangering losses and risk of human life can be significant. Therefore, it is critical to find ways to improving the durability and reliability of welded joints [6]. Poor weld characteristics and fatigue failure remain among the most common causes of welded structural failure in construction and mining equipment, railways, ships, agricultural machinery, bridges, and off-shore equipment, resulting in significant economic losses. During operation, structural members and components in these structures are constantly subjected to variable-amplitude loading, [7].

Dissimilar joint of low-alloy ferritic steel and austenitic stainless steel have been widely used in many industries. [8] studied the joining of A240 TP316 austenitic stainless steel and A387 Gr.11 low-alloy ferritic steel using the GTAW process with constant and pulsed currents. Two types of filler metals namely, ER309L and ERNiCr-3, were used in this investigation. The microstructure of the dissimilar weldment was characterized by conventional metallography using optical microscopy scanning electron microscopes and by energy-dispersive spectroscopy (EDS). The mechanical properties of test samples were evaluated using tensile, Charpy impact and microhardness tests. The findings showed that samples welded with pulsed current exhibit relatively higher impact energies mainly due to lower heat input and creation of intense mixing in the welding pool. Consequently, the formation of undesirable microstructural features such as carbon-depleted zone, transmission region and unmixed zones was reduced in the pulsed-current welded specimens. Among all the filler metals used, the nickel-based filler metal was found to be more suitable because it limits, the migration of carbon into the welding pool and reduced the risk of transition-region formation compared with the other filler metals.

METHODOLOGY

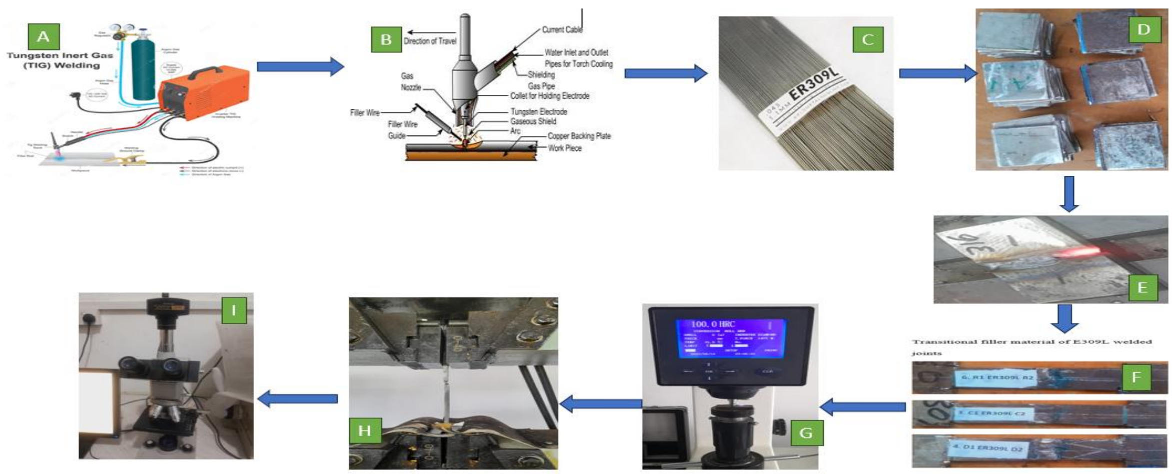

Figure 2.1 Block Diagram of Gas Tungsten Arc Welding for ER309L Filler Materials Joining Experimental Set Up System (Tungsten inert gas welding station setup; working principles of TIG Welding Equipment; Transitional filler material of ER316L; samples of AISI 1010LCS/ASS304 Preparations; Single butt joint welded; Transitional filler material of E309L welded joints; Digital B Rockwell Hardness Testing Machine; tensile test machine; and Microscope Digital Camera 14MP mode of MU1400 USB2.0 DC 5V 250mA)

Table 2.1 Mechanical Properties of AISI1010 LCS

Mechanical Properties	Metric	Imperial
Ultimate Tensile Strength	36 5MPa	53ksi
Yield Tensile Strength	365 MPa	44 ksi
Yong's Modulus(E)	190-210Gpa	27,500-30,400ksi
Elongation at Break	20%	
Bulk Modulus (K)	140Gpa	20,300ksi
Shear Modulus	80Gpa	11,600ksi
Poisson's Ratio(V)	0.27-0.30	
Brinell	105	105
Density	7870 kg/m3	491Ib/ft3

2.1.3 Chemical Composition of AISI1010 LCS

AISI1010 steel is low carbon. Low-carbon steels generally contain a relatively small percentage of carbon, and AISI 1010 typically contains about 0.08% to 0.13% carbon by weight. Due to its excellent weldability and suitability such as drilling, tapping, grinding, punching, and machining operations, it is widely used as a general-purpose steel. However, heat dealing has petite upshot on AISI1010 steel because to its low carbon content, although it may be case-hardened to improve surface hardness. In addition to carbon, AISI 1010 contains small amounts of manganese, sulphur, phosphorus and silicon. It may also contain trace residual elements such as nickel and chromium, but these are not present in significant amounts. The alloying elements in AISI 1010 help for the required chemical and mechanical properties. Since AISI 1010 does not contain enough chromium or nickel, corrosion resistance compared with stainless steels was lesser.

Table 2.2: Chemical Composition of AISI1010

Element	Chemical Symbol	Content min (%)
Carbon,	C	0.13
Iron	Fe	99.62
Manganese,	Mn	0.60
Phosphorous,	P	0.04
Sulfur	S	0.05

Table 2.3 Physical Properties of AISI1010LCS

Physical Properties	Metric
Density	7.85 g/cm^3
Colour	Gray

Table 2.4 Thermal properties of AISI 1010

Thermal Conductivity	29 BTU/h·ft·°F
Specific Heat Capacity (Cp)	0.107 BTU/lb·°F
Coefficient of Thermal Expansion (αL)	6.78×10-6 1/°F

Table 2.5 Electrical Properties of AISI1010

Electrical Conductivity	2.12×106 S/ft
Electrical Resistivity	4.69×10-7 Ω·ft

Table2.6 show Chemical Composition Austenitic Stainless Steel (AISI304) (wt %)

Element symbol	304
Carbon C	0.08%
Chromium Cr	18-20%
Nickel N	8-12%

Manganese M	2%
Silicon Si	1%
Phosphorus P	0.045%
Sulfur S	0.03%
Nitrogen N	0.0-10.11

Table 2.7 Mechanical properties Austenitic Stainless Steel (AISI) Type 304

Property	Metric	Imperial
Tensile Strength	515-620MPa	75,000-90,000psi
Yield Strength	205-205-310MPa	30,000-45,000 psi
Elongation	40-60%	
Hardness (Rockwell B)	85-95	

Table 2.8 Physical properties of 304 stainless steel

Property	304
Density	8.00 g/cm3
Modulus of Elasticity, psi	193 GPa
Melting Point	1450 °C
Thermal Conductivity	16.2 W/m.K
Thermal Expansion	17.2 x 10-6/K"
Electrical Resistivity	0.72 x 10-6 Ω.m
Color silvery bright and reflective.	

Table 2.9 show ER309L Chemistry (%)

Element	ER309L
C	0.01
Mn	1.88
Si	0.42
Mo	0.08

Element	ER309L
Cr	23.03
Ni	13.74
Cu	0.11
P	0.02
S	0.001
N	0.062

Table 2.10 show ER309l of Mechanical Properties.

Tensile strength (psi)	87,200
Yield strength (psi)	58,000
Elongation in 2"(%)	40

Table 2.11 show ER-309L Filler wires Specification

Classification**:** AWS A5.9 ER-309L, A5.9M:2006
Soft Wire Diameter Range**:** 0.06mm – 2.30 mm
Hard Wire Diameter Range: 0.30mm – 3.00mm
Diameter: .035”, .045”, 1/16”, 3/32”, 1/8”, 5/32”
Length: 36" (914mm) Customized
Materials: ER-309L Stainless Steel
Form: Wires, Filler Wires, Coil Wires, Welding Wires

2.1.4 Transitional filler material of ER309L

With an average carbon content of.02%, ER309L is similar to ER309 but it produces weld deposit with high resistance to intergranular corrosion caused by carbide precipitation. ER309L is excellent for buttering passes and overlay work. commonly weldment of dissimilar metals, such as stainless steel to mild steel or low-alloy steel, and for applications where ER309 welding wire is normally recommended.

2.2.5 TIG welding

TIG/GTAW arc weldment process that uses a welding power source, of inert shielding gas and a TIG torch. Electrical energy is supplied from the power source through the TIG torch to a non-consumable tungsten electrode mounted in the torch assembly. An electric arc is then established between the tungsten electrode and the workpiece, the tungsten electrode and the weld zone are protected from atmospheric contamination by an inert shielding gas, usually argon, helium or an argon-helium mixture. The electric arc generates very high temperatures, which produce a concentrated heat source at the joint area. This localised heat melts the edges of the base metals to form a weld pool, which solidifies to create a permanent joint.

Depending on the joint design, material thickness and welding requirements, the process may be carried out with or without filler metal. According to [9], TIG welding maintains an arc between a tungsten electrode and the workpiece within an inert atmosphere. Depending on the weld preparation and the thickness of the work-piece, TIG welding may be performed with or without filler metal. The filler metal may be introduced manually or automatically depending on the type of welding process being used. The process may be manual, semi-mechanised, fully mechanized or automatic. The welding power source may supply either direct current (DC) or alternating current (AC) [10]. The GTAW station consists of four major components: the welding power supply, often referred to as the welding machine; the welding torch, commonly called the TIG torch; the work clamp, sometimes referred to as the ground clamp; and the shielding gas cylinder. These components are connected by various hoses and cables that enable the welding system to operate effectively [11].

2.2.6 Experimental procedure

Two steel samples, namely Low-Carbon Steel AISI 1010 and Austenitic Stainless Steel 304, were subjected to elemental composition analysis using the Angstrom V-950 spectrometer. The analysis was conducted at Tema Steel Company Limited Ghana and the findings are presented in this report. The elemental analysis produced accurate and reliable results, confirming the chemical conformations of the two steel samples. The results also demonstrate the suitability of the Angstrom V-950 spectrometer for material identification and quality control applications. The AISI 1010 LCS and AISI 304 ASS plates were measured and cut to the required sample dimensions of 100 mm × 50 mm × 5 mm using a 9-inch angle grinder fitted with a cutting disc at the Welding and Fabrication Department Workshop of Krobea Asante Technical Vocational Institute. A 30-degree single V-groove was then prepared on the specimens. Before welding, the specimens were cleaned to remove dust, oil and other surface contaminants that could affect the molten weld pool. The plates were then tack-welded into position to achieve the required joint alignment before final welding.

2.2.7 Method for dumbbell preparation of AISI1010LCS/ASS304 (ASTM D412 TYPE A)

The ASTM D412 standard test method is used to determine the tensile properties of vulcanised rubber and thermoplastic elastomers under controlled loading conditions. The test measures properties such as tensile strength, elongation and permanent deformation after the applied load were removed. These measurements are used to evaluate the elasticity and mechanical performance of the material.

ASTM D412 is commonly used in industries such as automotive, aerospace, medical and manufacturing, where rubber and elastomeric materials must meet specific strength and elongation requirements. It is an important tensile testing method for product development, material selection and quality control. However, the specimen's weldment in TIG and amalgamated were done.

2.2.8 PNE61-series Main characteristics

- IGBT inverter.
- High reliability and excellent welding performance.
- Wide range of supply voltage.
- Multiple adjustable parameters and argon arc operation modes.
- Visual and easy to operate.
- RS-485 communication socket match RC-6, RC-7 remote controller
- Realization of remote setting and supervision by TIME TWPM welding process management system
- Cellulose welding is optional

Table 2.15 Technical parameters of PNE61 weldment.

Model	WS-400
Company type	PNE61-400
Rated input voltage(V)	3 phase 380V±15% 50~60Hz
Rated Input capacity (KW)	17
No-load voltage (V)	76±5%
Output current adjusting range(A)	5~410
Slope up time (s)	0.1~99.9
Pre-flow time (s)	0~13
Post-flow time (s)	0.1~50
Ignition time (s)	0.01~1s

Duty cycle (40℃)	60%
Efficiency (η)	85%
Power factor (cosΦ)	0.93
Insulation grade	F
Case protection grade	IP23S
Cooling	Wind
Dimensions (mm)	560×300×530
Net weight (kg)	34

2.2.10 Tensile Test

For tensile testing, the machine is fitted with replaceable grips that can hold both flat and cylindrical specimens. Bending test accessories are mounted in the lower section of the machine. After the data are processed by the control unit, the experimental results are displayed on the digital testing machine's monitor. Nine butt-joint specimens, grouped into three sample sets, were fabricated using the TIG weldment process were used for the experiment. The tensile tests were conducted using a WAW-1000B universal tensile testing machine. Each specimen was mounted between the upper and lower grips of the tensile testing machine and loaded in tension until failure.

2.2.11 Hardness Test

Scholars all of it designated the sequences of dent methodological test amid the active and effectual dent hardness handling test. The writers adopted [12] measurement charactered procedural for the indentation. However, the practical-strength was pended for an exact hiatus of time and after that force discount which returns to the prior force level. This work done, the used force of 15ogf in 10s. An experimental configuration of a specimen in the digital B Rockwell hardness testing apparatus was used [13].

2.2.12 Impact Strength Test

The notched specimens were placed on the HSM 55 Pendulum impact tester (300J), a digital impact testing machine with a specimen-supported anvil near the base. The pendulum was raised to the required height and secured in its initial position by a catch It was then released to strike the specimen with the specified impact energy. The specimens were observed during and after the test to assess their fracture behavior and bending angle. The 300 J impact testing machine and the bent angle of the specimen subsequently impact is exposed in the relevant figure.

2.2.13 Metallographic Testing

The MP-2B Grinder Polisher was used to prepare metallographic samples from the welded specimens. The MP-2B grinder-polisher was used to prepare metallographic samples from the welded specimens. The samples were pre-ground, polished and etched before metallographic examination. For the AISI 1010 and ER309L welds, the specimens were etched using a solution containing 45 g ferric chloride, 9 g ammonium chloride, 150 mL hydrochloric acid and 75 mL distilled water. For the AISI 304 austenitic stainless-steel welds, the specimens were etched using a solution of 95% ethanol and 5% nitric acid. The microstructural scrutiny was carried out in the laboratory using an AmScope MU1400 digital microscope camera with a 14 MP Aptina colour CMOS sensor at ×10 magnification. The preparation of the metallographic specimens began with the sectioning process. A power hack saw was used to cut the specimens to a suitable size that including the weld metal, HAZ and base metal regions, to obtain representative specimens from the bulk welded samples. After sectioning, the samples were ground, polished and etched before their microstructures were scrutinized underneath a microscope. Grinding and polishing were carried out to remove cutting marks and produce a mirror-like surface, while etching revealed the grain boundaries under the microscope. After preparation, the specimens had bright, mirror-like polished exteriors that were free from visible scratches. Microstructural images of the samples were observed under the microscope at selected regions of interest.

3.0 RESULTS AND DISCUSSSION

3.1 Tensile Test Result and its Analysis of ER309L, Weld of AISI1010LCS/AISI304ASS

1. Extensometer gauge length: 50 mm
2. Tensile strength: 145.1 MPa
3. Original gauge length: 80 mm
4. Yield force: 44.4 KN
5. Lower yield point: 44.29 KN
6. Upper yield strength: 141 MPa
7. Lower yield strength: 141 MPa
8. Diameter: 20 mm
9. Maximum force: 45.6 KN

3.1.2 Calculations:

1. Area calculation: Area = π × (diameter/2) ^2 = π × (20/2) ^2 = approximately 314.16 mm^2
2. Yield strength calculation: Yield strength = Yield force / Area = 44.4 KN / 314.16 mm^2 ≈ 141.3 MPa.

3.1.3Analysis:

1. Tensile strength: The material exhibits a tensile strength of 145.1Mpa
2. Yield strength: The material has a yield strength of approximately 141 Mpa (both upper and lower)
3. Material behaviour. The close value of upper besides lower yield strength suggests a relatively stable plastic deformation behaviour.

3.1.4 Comparison of Tensile strength vs. Yield strength of the sample

Tensile strength vs. Yield strength: The tensile strength is slightly higher than the yield strength, indicating a moderate level of strain hardening. The tensile test results indicate that the steel sample with ER309L filler metal exhibits a tensile strength of 145.1 MPa and a yield strength of 141 MPa. The material's behavior suggests ductility and stability during plastic deformation.

Table 3.1 shows the result of the Steel tensile test Specimen for AISI100/AISI304 sample, using (ER309L) transitional filler material

extensometer gauge length (mm	original gauge length (mm)	yield force on （KN）	upper yield strength (Mpa	diameter （mm)
50	80	44.29	141	20
tensile strength (Mpa)	final gauge length after fracture (mm)	lower yield point （KN）	lower yield strength (Mpa)	maximum force (kn)
145.1		44.29	141	45.6

3.1.5 showTensile Test Data Result Analysis of ER309L, Weld of AISI1010LCS/AISI304ASS sample

1. Extensometer gauge length: 50 mm
2. Tensile strength: 167.8 MPa
3. Original length: 80 mm
4. Yield force: 50.59 KN
5. Lower yield point: 50.59 KN

6. Upper yield strength: 161 MPa
7. Lower yield strength: 161 MPa
8. Diameter: 20 mm
9. Maximum force: 52.7 KN

3.1.6. Calculations

1. Area calculation: Area = π × (diameter/2) ^2 = π × (20/2) ^2 = approximately 314.16 mm^2
2. Yield strength calculation: Yield strength = Yield force / Area = 50.59 KN / 314.16 mm^2 ≈ 161 MPa (matches given values)

Analysis:

1. The material exhibits a tensile strength of 167.8 MPa.
2. Yield strength: The material has a yield strength of 161 MPa (both upper and lower).
3. Material behavior: The close values of upper besides lower yield strength suggest a relatively stable plastic deformation behavior.

3.1.7 Comparison of Tensile Strength vs. Yield Strength of the Sample

1. Tensile strength vs. Yield strength: The tensile strength is slightly-higher than the yield strength, indicating a moderate level of strain hardening.
The tensile test results indicate that the steel sample with ER309L filler metal exhibits a tensile strength of 167.8 MPa and a yield strength of 161 MPa. The material's behavior suggests ductility and stability during plastic deformation, with a moderate level of strain hardening.

Table 3.2 shows the result of the Steel tensile test Specimen for AISI100/AISI304 sample using ER309L transitional filler material

extensometer gauge length (mm	original gauge length (mm)	yield force on （KN）	upper yield strength (Mpa)	Diameter （mm)
50	80	50.59	161	20
tensile strength (Mpa)	final gauge length after fracture (mm)	lower yield point （KN）	lower yield strength (Mpa)	maximum force (kn)
167.8		50.59	161	52.7

3.1.8 showTensile Test Result Data Analysis of ER309L, Weld of AISI1010LCS/AISI304ASS sample

1. Extensometer gauge length: 50 mm
2. Tensile strength: 176.1 MPa
3. Original gauge length: 80 mm
4. Yield force: 46.62 KN
5. Lower yield point: 46.62 KN
6. Upper yield strength: 148.4 MPa
7. Lower yield strength: 148.4 MPa
8. Diameter: 20 mm
9. Maximum force: 55.3 KN

Table 3.3 shows the result of Steel tensile test Specimen for AISI1010/AISI304 sample using ER309L transitional filler martial

extensometer gange length (mm	original gauge length (mm)	yield force on (KN)	upper yield strength (Mpa)	Diameter (mm)
50	80	46.62	148.4	20
tensile strength (Mpa)	final gauge length after fracture (mm)	lower yield point (KN)	lower yield strength (Mpa)	maximum force (kn)
176.1		46.62	148.4	55.3

3.1.9 shows Comparison of Transitional Filler Metals for AISI 304 ASS and AISI 1010 LCS of **ER309L**

1. Tensile strength range: 145.1 MPa to 176.1 MPa
2. Yield strength range: 141 MPa to 161 MPa
3. Material behavior: Ductility and stability during plastic deformation, with moderate to significant strain hardening.

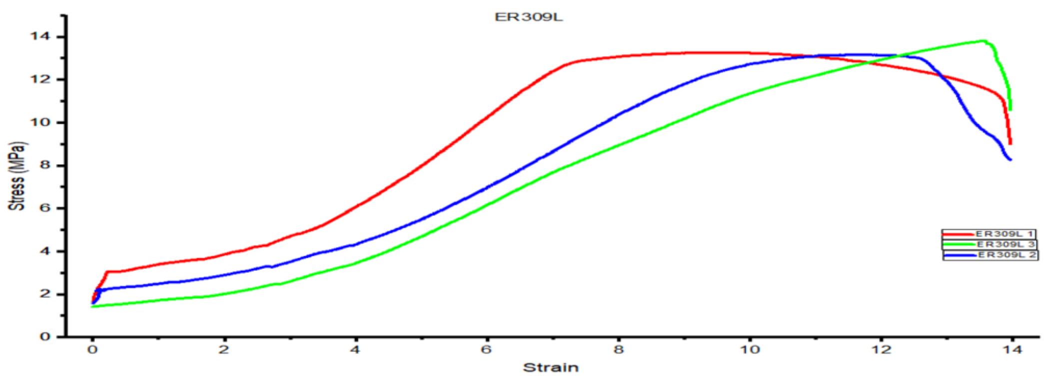

Fig 3.1 show ER309L Material behavior ductility and stability during plastic deformation, with moderate to significant strain hardening.

Table3.4: Indentation values of Rockwell hardness (HRC) on ER309L of AISI1010LCS/ AISI304ASS (HAZ)

SAMPLE/HARDNESS	HRC	HRC	HRC	HRC	HRC	HRC	AVERAGE
AISI1010LCS	35.20	30.60	30.70	30.00	29.50	52.70	34.79
AISI304ASS	56.90	58.70	60.60	55.40	61.00	57.61	58.37

3.1.10 HRC VALUES OF AISI 1010 LCS/AISI 304 ASS (HAZ) OF ER309L ANALYSIS.

AISI 1010 LCS HRC values: 35.20, 30.60, 30.70, 29.50, 52.70
Average HRC: 34.79
AISI 304 ASS HRC values: 56.90, 58.70, 60.60, 55.40, 61.00, 57.61
Average HRC: 58.37
AISI 1010 LSS/AISI 304 ASS (HAZ) The HRC values show significant variation, ranging from 29.50 to 52.70. AISI 304 ASS. The Average HRC value is 34.79, indicating a relatively lower hardness in the HAZ.
The HRC values are consistently high, ranging from 55.40 to 61.00.
The average HRC value is 58.37, indicating a high hardness of the base material.

3.1.11 Microstructure Analysis of the HAZ of AISI1010LCS/ AISI304ASS

Microstructure is one of many techniques that can be used to examine a material's properties. Due to phase changes that occur as a result of welding a joint, weld specimens can have large variations in microstructure across the specimen.

3.1.12 fracture hardness

The rapture of ER309L-Filled Dissimilar GTAW Joints Between AISI 304 Stainless Steel and AISI 1010 Low-Carbon Steel, alarmed earlier on the outward body layer during manufacturing resistance of material to plastic deformation. However, the positioned layer boundaries of grain and its arrangements star, the lighter the individual crystal grains, the harder the material becomes because metal material expanding the hardness but also makes it more brittle, and it in confirmation to [13].

3.1.13 Microscope Digital Camera with magnification ×10 AISI1010LCS, AISI304ASS, HAZ AND ER309L

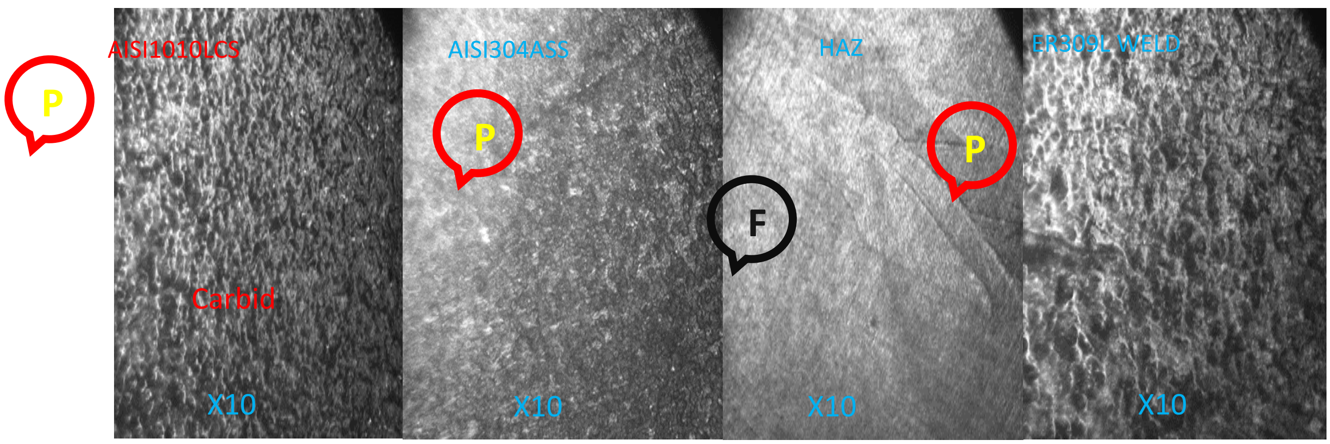

Figure 3.2 shows the microstructure of AISI1010LCS, AISI304ASS, and HAZ with ER309L

From Figure 3.2 shows the microstructures captured with a digital microscope camera at ×10 magnification. The AISI 1010 low-carbon steel region exhibits an assortment of ferrite and pearlite phases. The incidence of harder phases may be associated with carbide precipitates within the microstructure. The AISI 304 austenitic stainless-steel region also suggests the presence of harder phases, possibly due to carbide precipitation or phase transformation within the welded region. The HAZ of the AISI 1010 LCS/AISI 304 ASS joint and the ER309L weld metal also show mixed microstructural features, including ferrite and pearlite phases.

4.0 CONCLUSIONS

In this investigation, ER309L filler material was used to join AISI 304 ASS and AISI 1010 low-carbon steel using the GTAW process. The impact energy values indicated variations in toughness and ductility across the welded specimens. The hardness profile of the ER309L butt joints also showed variations across the HAZ, which will likely trait to residual stresses settled during temperature influenced after weldment. For the AISI 1010 LCS HAZ, the HRC values showed significant variation, ranging from 11.90 to 60.60, with an average hardness value of 33.44 HRC. For the AISI 304 ASS HAZ, the HRC morals were more consistent, ranging from 57.20 to 63.60, with an average hardness value of 60.67 HRC. This indicates that AISI 304 ASS had a significantly sophisticated-hardness than AISI 1010 LCS, respectively. The weldment microstructure showed the presence of ferrite and pearlite, which may insert to the mechanical behaviour of the weldment-joint.

REFERENCES

[1] Abioye, T.E., Ariwoola, O.E., Ogedengbe, T.I., Farayibi, P.K., Gbadeyan, O.O., 2019. Effects of welding speed on the microstructure and corrosion behavior of dissimilar gas metal arc weld joints of AISI 304 stainless steel and low carbon steel, Materials Today Proceedings 17, pp. 871–877.

[2] Kang, J.Y., Kim, D.I., Lee, H.C., 2009. Texture Development in Low Carbon Sheet Steels for Automotive Application. In: Haldar, A., Suwas, S., Bhattacharjee, D. (eds) Microstructure and Texture in Steels. Springer, London. https://doi.org/10.1007/978-1-84882-454-6_5

[3] Vashishtha, H., Taiwade, R., Sharma, S., Marodkar, A., 2019. Microstructural and Mechanical Properties Evolution of Bimetallic Cr-Ni and Cr Mn-Ni Stainless Steel Joints. Metallography, Microstructure, and Analysis 8 pp. 359-369. https://doi.org/10.1007/s13632-019-00549-w.

[4] Awad, I., Khedr, M., Mahmoud, T.S., Abdel-Aleem, H., Hamada, A., 2021. Study on the Mechanical Performance of Dissimilar Butt Joints between Low Ni Medium-Mn and Ni-Cr Austenitic Stainless Steels Processed by Gas Tungsten Arc Welding. Metals 11, 1439.

[5] Bahrami, A., Helenbrook, B., Valentine, D., Aidun, D., 2016. Fluid flow and mixing in linear GTA welding of dissimilar ferrous alloys. International Journal of Heat and Mass Transfer, 93, 729-741. https://doi.org/10.1016/J.IJHEATMASSTRANSFER.2015.10.058.

[6] Huang, Y., Huang, J., Zhang, J., Yu, X., Li Q., Wang, Z., 2021. Microstructure and corrosion characterization of weld metal in stainless steel and low carbon steel joint under different heat input. Materials Today Communications 29, pp. 102948.

[7] Eshkabilov, S., Ara, I., Sevostianov, I., Azarmi, F., Tangpong, X., 2020. Mechanical and thermal properties of stainless-steel parts, manufactured by various technologies, in relation to their microstructure. International Journal of Engineering Science 159, pp. 103398.

[8] Khedr, M., Elsayed, M., Jaskari, M., Abdel-Aleem, H.A., Gaafer, A.M., Hamada, A, 2024. Effect of building orientation on weld characteristics of additively manufactured 316L stainless steel: Microstructure and mechanical properties. Materials Science & Engineering A 913, 147086.

[9] Maurya, A.K., Pandey, C., Chhibber, R., 2021. Dissimilar welding of duplex stainless steel with Ni alloys: A review, International Journal of Pressure Vessels and Piping 192, pp. 104439.

[10] Khedr, M., Awad, I., Jaskari, M., Ali, M., Abdel-Aleem, H., Mahmoud, T.S., Hamada, A., 2023. Microstructural Evolution and Mechanical Performance of Two Joints of Medium-Mn Stainless Steel with Low-and High-Alloyed Steels. Materials 16, 1624.

[11] Mvola, B., Kah, P., Martikainen, J., Suoranta, R., 2015. State-of-the-art of advanced gas metal arc welding processes: Dissimilar metal welding. Proceedings of the Institution of Mechanical Engineers, Part B: Journal of Engineering Manufacture 229(10), pp 1694-1710. doi:10.1177/0954405414538630

[12] WANG Yun, BAIDOO Philip*, XU Zhenying, Wu Junfeng (2018) Study on fatigue crack growth performance of EH36 weldments by laser shock processing. (J). surfaces &interface, 2018, 147; 12-1. 252. SCI. (https://doi.org/10.1016/j.surfin.2018.10.009)

[13] BAIDOO Philip (2020) the comparative study of the sway of effect pulse energies of pathways on AHSS-DP 350/600 and simulation. (J) Determinations in Nanomedicine & Nanotechnology (DNN), published; 2020, volume 1, Issue 5. (1(5). DNN.000525.2020)